Eur. Phys. J. Spec. Top. (2021) 230:673–688
https://doi.org/10.1140/epjs/s11734-021-00021-3

THE EUROPEAN PHYSICAL JOURNAL SPECIAL TOPICS

Review

Initial fluctuations and power spectrum of flow anisotropies in relativistic heavy-ion collisions

Shreyansh S. Dave[1,a], P. S. Saumia[2,b], and Ajit M. Srivastava[3,c]

[1] The Institute of Mathematical Sciences, Chennai 600113, India
[2] Bogoliubov Laboratory of Theoretical Physics, JINR, 141980 Dubna, Russia
[3] Institute of Physics, Bhubaneswar 751005, India

Received 26 June 2020 / Accepted 10 February 2021 / Published online 19 April 2021

Abstract Flow has emerged as a crucial probe for the properties of the thermalized medium produced in relativistic heavy-ion collisions. The evolution of initial state fluctuations leaves imprints on the power spectrum of flow coefficients. Therefore, flow coefficients are a crucial probe of initial state fluctuations arising from the parton distributions of the colliding nuclei. This has a very strong correspondence with the physics of power spectrum of cosmic microwave background radiation (CMBR) anisotropies which directly probes initial inflationary fluctuations. Much work has been done to probe these interesting interconnections, in particular, in developing techniques for the measurements of higher flow coefficients. We present a short review of these developments. The effect of initial magnetic field on these features will also be reviewed. All this acquires special importance in view of upcoming electron-ion collider which will directly probe initial parton distribution of the colliding nucleus.

1 Introduction

Relativistic heavy-ion collision experiments (RHICE) have provided us with a remarkable opportunity of investigating properties of strongly interacting matter under extreme conditions of temperature and/or baryon density. This complements our efforts to understand perturbative aspects of quantum chromodynamics (QCD), the theory of strong interactions, with ultra-high-energy colliders, extending it in the regime where non-perturbative aspects play crucial role. Indeed, entire QCD phase diagram is now subject of experimental investigation with issues like phase transition, critical point, etc., being examined in the light of experimental data as well as theoretical predictions using non-perturbative techniques like lattice gauge theory, effective field theory, etc. All this has allowed us to make significant progress in our overall understanding of QCD. At the same time, we are able to study, under experimentally controlled situations, those aspects of our universe which are beyond direct reach of experiments.

High baryon density regime of QCD is being probed by the beam energy scan program of RHIC, and will be the main focus of upcoming facilities FAIR and NICA. These directly provide us with inputs for understanding the behavior of matter in important astrophysical objects such as neutron stars, and possibly the behavior of stars undergoing collapse to black holes during their last stages. Exotic phases of QCD have been postulated in the QCD phase diagram at very high baryon densities such as color flavor locked (CFL) phase, crystalline superconductivity phase, 2SC phase, etc. which could occur in the interiors of such objects [1]. Possibilities are being explored of detecting such phases in heavy-ion collision experiments. Even a somewhat more conventional, nucleonic superfluidity phase, which is believed to be crucial for understanding pulsar glitches, may become accessible in relatively low-energy heavy-ion collisions [2].

A completely different regime in the QCD phase diagram provides a direct insight into the very early stages of our universe when its age was about few microseconds. This is the regime of high temperature and very low baryon density. Ultra-relativistic collisions of heavy nuclei at RHIC and LHC have provided, and are continuing to provide invaluable data which have made qualitative changes in our understanding of this extremely important regime of QCD phase diagram. This is the regime in which lattice QCD simulations have provided extremely reliable calculations (compared to the high baryon density regime). A constant dialogue between lattice predictions and experimental observations have allowed reasonably reliable conclusions to be reached, e.g., the formation of quark-gluon plasma (QGP) phase of QCD in these experiments and the quark-hadron transition temperature. It has shown that quark-hadron transition in this regime of phase diagram is a crossover

[a] e-mail: shreyanshsd@imsc.res.in
[b] e-mail: saumia@theor.jinr.ru (corresponding author)
[c] e-mail: ajit@iopb.res.in

transition. The correspondence with the early universe phase certainly makes this regime very exciting.

Probably, the most important observation from the relativistic heavy-ion collision experiments is the measurement of so-called *elliptic flow* [3–6]. There have been many signals proposed for the observation of the quark-gluon plasma (QGP) phase of QCD in these experiments. Starting with the J/ψ suppression, to strangeness enhancement, jet quenching, photons/dileptons are some of the important signals which have been thoroughly analyzed and compared with data with varying degrees of success in providing a clean signal for QGP formation. Certainly, all the signals together, including elliptic flow, have allowed us to be confident that indeed the QGP phase has been produced in these experiments. At the same time, it seems fair to draw attention to elliptic flow (flow in general) in providing us with qualitatively new features of the thermalized medium produced. Two points can be made to support this claim, the first one being thermalization. All other signals require quantitative details to distinguish between the effects of a thermalized medium from the effects of a dense medium which may be out of equilibrium. However, elliptic flow most directly probes the equilibrium behavior of the medium. As we will explain below, whatever be the anisotropies in the initial spatial distribution of energy density, in an ultra-relativistic collision where initial transverse velocity is negligible, momentum anisotropies can only arise from development of anisotropic pressure gradients. Thus, a degree of equilibration is necessary, so that well-defined distribution of pressure can arise. Though there have been efforts to explain the observed momentum anisotropies in terms of anisotropic diffusion through a dense medium, without assuming equilibrium, such efforts have not met much success in accounting for the wealth of data on elliptic flow.

The second point because of which elliptic flow needs special mention is the qualitatively novel behavior of QGP it has revealed, way beyond any theoretical expectation. All other signals have only aspired to probe the standard picture of QGP as a thermalized gas of deconfined quarks and gluons. Elliptic flow has directly probed a very important transport coefficient, namely η/s, the shear viscosity-to-entropy density ratio. The experimental data are consistent with hydrodynamic simulations only with very small values of η/s, very close to the lowest limit $1/4\pi$ [7]. This is the smallest value of all known liquids, making QGP in these experiments as the most ideal liquid ever produced. This was certainly totally unexpected. Indeed, it is even contrary to the original spirit of the hypothesis of QGP where one argued for the existence of a weakly interacting deconfined gas of quarks and gluons at very high temperatures based on the asymptotic freedom of QCD. Instead, what one is seeing is that at the temperatures produced in these experiments, QGP is far from being an ideal gas (which should have large mean free path, hence large shear viscosity), but is behaving like a strongly interacting/correlated system.

It is then not surprising that elliptic flow, and flow in general has taken, in some sense, a center stage in the investigation of QGP in RHICE [8,9]. A very important realization in this regard was about the importance of initial state fluctuations in energy density. Due to random phase space distributions of nucleons (and partons within) inside colliding nuclei, the resulting initial medium necessarily had inhomogeneities in the transverse plane. It was well recognized that in calculations of elliptic flow v_2, as well as certain higher flow coefficients (namely v_4, v_6, and very occasionally v_8) in a non-central collision, there are uncertainties arising from the error in defining the axes of the event plane due to these fluctuations. Many investigations were carried out on these issues and techniques were developed to take care of these effects [10–14]. It was also recognized that these flow coefficients may have small non-zero values even in central collisions due to these initial fluctuations. It is interesting that despite this recognition of effects of fluctuations, no attention was paid to the other flow harmonics. In particular, odd flow coefficients were completely neglected.

A very different view on these initial state fluctuations was initiated by some of us in a series of papers [15,16]. The QGP, produced in RHICE, has initial energy density fluctuations. Because of presence of inside–outside pressure gradient, it expands hydrodynamically, therefore cools down, and reaches quark-hadron transition temperature, where QGP-to-hadron crossover transition occurs. These hadrons further evolve, and first chemically, then thermally freeze out, and finally reach the detectors carrying certain momentum distribution in the transverse plane. This momentum distribution of hadrons carries imprints of the initial state fluctuations and the properties of medium. Indeed, in discussions of heavy-ion collisions, it is often mentioned in popular terms that attempts to learn about the phase of matter in the early stages from the observations of hadrons are similar to the attempts to understand the early stages of the universe from the observations of the cosmic microwave background radiation (CMBR). The surface of last scattering for CMBR is then similar to the freezeout surface in RHICE. The last scattering surface represents the time when protons and electrons 'recombine' and the universe becomes neutral, so that photons can free stream through the universe. In refs.[15,16], such qualitative statements were extended to a deeper level of correspondence between flow fluctuations in RHICE and the CMBR fluctuations in the universe. Following the successes of the analysis of the CMBR anisotropy power spectrum in providing crucial information about initial inflationary density fluctuations, it was argued in these works that flow coefficients should be used as a probe for identifying initial state fluctuations in RHICE, thereby providing crucial information about initial nucleon/parton distributions. Thus, initial fluctuations should not only be considered as providing errors in calculating certain flow coefficients for non-central collisions, rather they should be the main focus of study as a source of information about initial system

itself. From that point of view, central collisions became much more important, as a large peak at v_2 for non-central collisions becomes a distractor when the focus is only on the initial state fluctuations. For a central collision, all flow coefficients became important, including the odd flow coefficients. With that, it was argued in [15,16] that one should plot the power spectrum of all flow coefficients, with the entire plot providing crucial inputs on the initial state fluctuations, as well as their evolution.

It is now generally recognized that a large number of flow coefficients need to be studied which not only contain effects of initial fluctuations, but also important correlations arising from hydro evolution. The subject of this short review is to provide developments in this area of study of flow coefficients with special focus on their power spectrum. We will begin in Sect. 2 with a brief recollection of the importance of elliptic flow and the effects of initial fluctuations on the determination of specific even flow coefficients in terms of resulting uncertainties in the determination of the event plane. Section 3 presents the new perspective on the initial state fluctuations as proposed in Refs. [15,16] emphasizing the importance of power spectrum of flow coefficients. Here, we will draw correspondence with the power spectrum of CMBR anisotropies and discuss possibilities of similar features, such as CMBR acoustic peaks in the flow power spectrum. Here, we discuss results from several investigations where general study of effects of initial state fluctuations on flow coefficients has been carried out. In Sect.4, we discuss some studies where correspondence with CMBR studies has been further explored. In Sect. 5, we discuss ways to isolate the effects of initial state fluctuations from the effects of hydrodynamical evolution. For this, we present results of magnetohydrodynamical evolution which show qualitative patterns on the power spectrum of flow coefficients in the presence of very strong magnetic fields. As the magnetic field is expected to be very strong only for very early stages (subsequently slowly decaying in time with medium effects included), such qualitative features of flow power spectrum can provide unique probe of the magnitude of initial state fluctuations which will be the subject of main focus for the upcoming electron–ion collider. We also discuss such qualitative patterns arising from any superfluid phase of QCD which could be produced in relatively low-energy collisions. In Sect. 6, we will conclude with discussion on new directions.

2 The elliptic flow

Elliptic flow has yielded the very useful and surprising information that the matter formed at RHIC behaves like an ideal liquid. In a simple picture, for non-central collisions, the interaction region is not circular in the transverse plane (xy-plane, as shown in Fig. 1), but rather has an elliptical shape. Once thermalization is achieved, the formed fluid has a thermal pressure, which varies in space with maximum value at the center of the system and zero outside in vacuum. Clearly, the pressure gradient, in the transverse plane, will be larger along the semi-minor axis of the ellipse (taken to be the x-axis in Fig. 1). This forces the plasma to undergo hydrodynamic expansion at a faster rate in that direction compared to the semi-major axis (the y-axis in Fig. 1). Thus, particles reach the detectors with larger momenta along the x-axis than the y-axis. In other words, the spatial anisotropy gets transferred into momentum anisotropy due to hydrodynamical flow.

Clearly, the generation of elliptic flow depends crucially on the equation of state relating pressure to the energy density and transport coefficients, e.g., shear viscosity-to-entropy ratio η/s. Thus, the observed momentum anisotropy of the particle distribution can be used with hydrodynamical simulations to extract useful information about hydrodynamic flow at very early stages, thereby directly probing η/s and the equation of state of the QGP (usually taken from lattice results). It is important to note that elliptic flow gives probably the most direct estimate of the thermalization time. If thermalization is delayed by a certain time, the elliptic flow would have to build on a reduced spatial deformation and would come out smaller. The observations put an upper limit of about 1 fm on the thermalization time for ultra-relativistic collisions at RHIC and LHC energies. The experimental data seem to be in very good agreement with the prediction of almost ideal hydrodynamics pointing to a very low η/s of the QGP produced. This shows that the QGP does not behave as a weakly interacting quark-gluon gas as predicted by perturbation theory; rather, it behaves as a strongly interacting/correlated liquid. This is termed as strongly coupled QGP (sQGP), with a strong non-perturbative interactions/correlations.

Anisotropy in the transverse momentum distribution is captured by the flow coefficients which are the Fourier coefficients of the azimuthal momentum distribution of particles. We consider the Fourier series of the azimuthal distribution of fractional transverse momentum distribution [17]:

$$\frac{1}{\bar{p_T}}\frac{dp_T(\phi)}{d\phi} = \sum_{n=0}^{\infty}\Big(a_n\cos(n\phi) + b_n\sin(n\phi)\Big). \qquad (1)$$

Here, $p_T(\phi)$ is the net transverse momentum in the angular bin at azimuthal angle ϕ and $\bar{p_T}$ is the angular average of the transverse momentum. The flow coefficients v_n are appropriate event averaged values of a_n and b_n. This definition of flow coefficients can be directly used for particle distributions as well as for the fluid momentum distributions in hydrodynamic simulations. We write the complete expansion here in the anticipation of the presence of fluctuations. In the absence of fluctuations, there is a reflection symmetry with respect to the reaction plane with which only the cosine terms survive. Generalization to transverse momentum p_T and rapidity y dependent flow coefficients $v_n(p_T, y)$ can be written straightforwardly in terms of differential distributions.

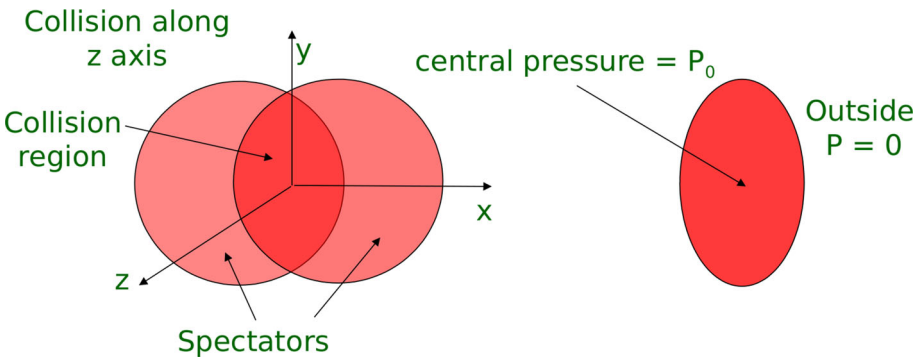

Fig. 1 Non-central collision leads to anisotropic interaction region in the transverse plane (xy-plane). With thermalization, one expects formation of an elliptical region of QGP in the transverse plane as shown in the right of Fig. 1. With anisotropic shape, and no initial transverse expansion, anisotropic pressure gradient implies that buildup of plasma flow will be larger in the x-direction than in the y-direction, leading to generation of elliptic flow

Even though we use the above definition for elliptic flow, very often, the flow coefficients are defined as the Fourier coefficients of the azimuthal distribution of the final particle number. These two quantities have a straightforward correspondence, since larger momentum in a bin in a fluid means a larger number of particles flowing into that bin. There are several methods of measuring the elliptic flow which is the second Fourier coefficient in the definition above. One method is to estimate the event plane, and then correlate the outgoing particles to this plane (for detail, see [18–20]). One could also use a two-particle correlation method to calculate the elliptic flow [21]. These two methods are equivalent, even though the latter does not need the determination of the event plane. However, it has been shown that both these methods have limitations due to event-by-event fluctuations as well as presence of non-flow correlations arising from resonance decays, jet fragmentation, etc. The picture of a smooth elliptical QGP region for a non-central collisions (as in Fig. 1) leading to elliptic flow is too simplistic. It was well known that initial state fluctuations are always present for any centrality. Due to these fluctuations, initial energy density distribution in the QGP region is non-homogeneous, e.g., as shown in Fig.2 for a central collision. Multiparticle cumulant expansions have been proposed to take care of these as well as detector effects [22]. It has been shown that there are improved methods involving multiparticle correlations like four particle cumulants and using the event plane determined from directed flow in a zero-degree calorimeter using three particle correlations of the spectators. These are insensitive to non-flow correlations as well as initial eccentricity fluctuations and hence measure elliptic flow effectively [23,24].

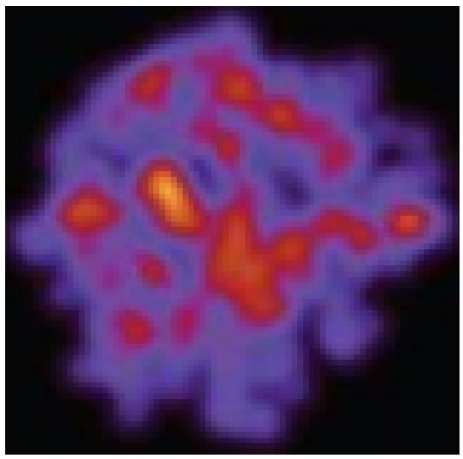

Fig. 2 With initial state fluctuations necessarily present, the resulting QGP region is not homogeneous; rather, it is lumpy as shown here for a central collision [25]

3 Correspondence with CMBR and the power spectrum of flow anisotropies

As we mentioned above, initial state fluctuations were initially discussed primarily in the context of determination of the event plane for elliptic flow calculations. Higher harmonics like v_4 and v_6 were seen as induced from v_2 and the eccentricity fluctuations as a higher order effect. However, no other flow coefficients, in particular, no odd harmonics, were discussed except a very early mention of the possibility of v_3 as well as v_4 due to initial deformation of the colliding nuclei rather than initial fluctuations [17]. The main reason for this was that the focus primary remained on non-central collisions to get elliptic flow which gave information about very important properties of QGP phase such as equation of state, viscosity, etc.

This view toward initial state fluctuations, as nuisance in getting the values of flow coefficients, was reversed in a series of papers by some of us [15,16] where these initial state fluctuations were made the center of attention. In these works, it was argued that initial state fluctuations are extremely important, originating from initial conditions, namely parton distributions inside the colliding nuclei. Thus, it was argued, in particular, that the central collisions are very impor-

tant. Non-central collisions retain their importance in getting strong signal for elliptic flow which probed equation of state, shear viscosity-to-entropy density ratio, etc. However, when one wants to learn about the initial state fluctuations, it is better to focus on central collisions, since the very large elliptic flow in non-central collisions tends to mask the effects of initial state fluctuations.

Figure 2 shows the typical initial energy density distribution for a central collision at the thermalization stage. As one can see, inhomogeneities of all scales are present, even in central collisions. With such lumpy initial energy density distribution, hydrodynamical evolution will be expected to lead to all flow coefficients becoming non-zero in general. Thus, all Fourier coefficients v_n should be of interest, including odd harmonics. The fact that the fluctuations and anisotropies in the final particle momentum distribution are directly related to fluctuations in the initial energy density distribution was further studied by various works [26–35]. There have been many discussions about various ways of appropriately quantifying the initial state fluctuations, e.g., see [28–30], so that the higher harmonics can be explained as a response to them. The higher flow harmonics are experimentally measured and their correspondence with different initial condition models were studied in [36–39]. Various flow observables including the ratios of different harmonics are shown to be largely determined by the initial state and hence helpful in studying the early stages [40]. It was also shown using viscous hydrodynamic simulations and other models that the different modes couple non-linearly during the evolution [41–43].

It is worth pointing out that this shift in focus to initial state fluctuations in ref.[15,16] was motivated from the realization of deep similarities between the physics of flow anisotropies in heavy-ion collisions and CMBR anisotropies in the universe. In this section, we will explain these motivations and develop this very intriguing correspondence in detail. To the skeptic reader, we mention that one main difference between the two system is the absence of gravity for heavy-ion physics. It will be easily seen below that it only affects overall scale of the resulting distribution of flow coefficients (the power spectrum of flow coefficients), without having any important effect on its shape. Another important difference is the presence of strong interactions in RHICE compared to the CMBR case where the physics at last scattering surface is governed by only electromagnetic interactions. As a result, equation of state of the matter is different in the two cases, but again, this is only expected to affect the quantitative features of the shape of the power spectrum.

As we mentioned, it has always been appreciated that the surface of last scattering of CMBR is in many ways like the freezeout surface for heavy-ion collisions. This is in the sense that for the former case, one can learn about the early universe from the CMBR photons from the surface of last scattering. In the same way, for heavy-ion collisions, one only gets hadrons from the freezeout surface. It is these hadrons which have to be analyzed to learn about the QGP system. The main ingredient in the new approach to flow coefficients relates to the fact that CMBR fluctuations originate from inflationary fluctuations during the initial stages of the universe. With CMBR power spectrum, one is able to learn about these initial inflationary fluctuations. In fact, the later stages of the universe (post-inflation) simply evolve these fluctuations. This evolution has to be understood, so that one can isolate the primordial inflationary fluctuations. In the same way, for heavy-ion collisions also, a power spectrum of flow coefficients should be used to probe directly the initial state fluctuations, with proper account of medium evolution effects.

This change of perspective naturally invites the use of techniques of CMBR analysis for heavy-ion case. For CMBR, the temperature anisotropies are analyzed using spherical harmonics, as appropriate for the surface of 2-sphere (the CMBR sky) [44]:

$$\frac{\Delta T}{T}(\theta,\phi) = a_{lm} Y_{lm}(\theta,\phi), \tag{2}$$

where T is the average CMBR temperature and ΔT is the fluctuation in the temperature from its average value. The coefficients of the expansion a_{lm}, corresponding to the spherical harmonic Y_{lm}, are degenerate in the argument m. When averaged over different values of m, these vanish due to isotropy of the universe. The variance of a_{lm} denoted by C_l (with suitable normalizations) is plotted with respect to l leading to the celebrated power spectrum of CMBR anisotropies [44]:

$$< a_{lm} >= 0 \quad , C_l \sim < |a_{lm}|^2 > . \tag{3}$$

The same technique was applied in [15,16] for analyzing particle momentum anisotropies, using lab fixed frame, in RHICE to probe the flow anisotropies. For RHICE, focusing on central rapidity region, one analyzes momentum anisotropies on a circle, requiring the use of the Fourier coefficients v_n. These should be distinguished from the conventional flow coefficients v_n which are defined with respect to the event plane. However, our purpose here is to develop a probe of initial state fluctuations and these v_n defined here serve this purpose. For relation between these flow coefficients and the conventional ones, see Ref. [16]. With a fixed lab frame, the event average values of these v_ns will all be zero due to rotational symmetry. We then use the variance of v_n, i.e., v_n^{rms} in analogy with C_l for CMBR:

$$< v_n >= 0, \quad v_n^{\rm rms} = \sqrt{< v_n^2 >}, \tag{4}$$

where $< v_n^2 >=< a_n^2 > + < b_n^2 >$; $< .. >$ denotes event average of the quantity, and a_n and b_n are the Fourier coefficients in Eq. (1). We point out here that a similar definition of power spectrum of flow coefficients was earlier proposed, though it was in the context separating flow and non-flow effects [45]. In view

of the correspondence with the CMBR power spectrum, the flow coefficients were defined in ref. [15] using the azimuthal distribution of $\Delta p_T(\phi)/(\bar{p_T}\Delta\phi)$ where $\Delta p_T(\phi) = p_T(\phi) - \bar{p_T}$ with $\bar{p_T}$ being the angular average of the transverse momentum p_T.

A plot of v_n^{rms} vs. n for a large range of n will provide the power spectrum of flow coefficients for relativistic heavy-ion collisions. The detailed structure of this plot for central collisions should reveal information about initial state fluctuations as well as their hydrodynamical evolution.

Several works later adapted CMBR analysis techniques more elaborately for the study of flow fluctuations using spherical harmonic expansion of the momentum distribution of particles including the pseudorapidity η [46–51]. They discuss the relation between the full angular power spectrum and flow coefficients. References [46,50] also show the Molleweid projection of the momentum distribution similar to the WMAP and COBE maps of the cosmic microwave background radiation, and propose that these maps can be used to study the non-flow fluctuations after subtracting out the collective effects. Using hydro simulations, maps of fluctuations of energy density and temperature in small phase space bins have been produced similar to CMBR maps [52].

With this important lesson from CMBR analysis tools for RHICE, the next step is to ask what important features of this power spectrum can be expected, and if at all there can be any similarities with the shape of CMBR power spectrum which is shown in Fig. 3. We will summarize the relevant parts of the physics of CMBR power spectrum below.

3.1 The essential features of the CMBR power spectrum

Figure 3 shows the CMBR power spectrum where l along the X-axis is related to the different wavelength modes of the temperature fluctuations on the CMBR sky. l could also be understood as $l \sim \pi/\theta$ where θ is the angular separation on the CMBR sky. The Y-axis corresponds to the power in each mode at the time of last scattering. The temperature fluctuations on the other hand are directly related to the density perturbations on the last scattering surface. These density perturbations have their origins in the early inflationary stage of the universe. During inflation, the universe expanded exponentially, stretching out the quantum fluctuations in the inflaton field to superhorizon scales. As inflation ends, reheating occurs converting these fluctuations into matter density perturbations. These perturbations evolve after inflation and eventually lead to structure formation during matter domination stage.

One of the important features of these density perturbations is their superhorizon length scales. In simple terms, for the universe, the horizon size = speed of light $c \times$ age of the universe t. The perturbations stretched out by the inflation start re-entering the horizon after the inflation owing to the faster expansion of the horizon scale ($\sim t$) as compared to the expansion of the universe ($\sim t^{1/2}$ in radiation dominated era or $\sim t^{2/3}$ in matter dominated era). As they enter the horizon, the perturbations start oscillating. In the matter dominated era, the perturbations 'grow' due to gravitational effects and oscillate. However, the scales larger than the horizon size at recombination stay as superhorizon modes in the CMBR temperature fluctuations on the last scattering surface. In Fig. 3, $l \sim 200$ represents the horizon at last scattering. The lower l modes represent the ones that are superhorizon. These are the scales unaltered by any causal physics before the recombination stage in the universe except for damping effects due to photon diffusion and remain as laid down by the inflationary fluctuations. Superhorizon fluctuations for universe do not oscillate (these are frozen). More importantly, they do not grow. That is, they are suppressed compared to the fluctuations which enter the horizon and grow by gravitational collapse.

Another important feature of the inflationary density perturbations is their coherence. As the fluctuations are stretched out of the horizon by inflation, they freeze out dynamically. This means that any mode which is frozen out remains as an oscillation in space, but not in time. As a result, when they re-enter, they enter with zero oscillation velocity (in phase), and hence, modes of same wavelength start evolving coherently everywhere leading to coherent acoustic oscillations.

The location of the first peak in the power spectrum represents the largest mode which has grown to its maximum at recombination and hence also tells us about the corresponding horizon scale. $l > 200$ represents the modes at the various stages of acoustic oscillations at the time of last scattering. The positions and the heights of the different peaks in the power spectrum carry important information about the contents of the universe until the time of last scattering.

3.2 Power spectrum of flow anisotropies

We will focus on two main features of the power spectrum in Fig. 3, namely the suppression of superhorizon modes and the acoustic oscillations. We will argue that similar physics is present for RHICE, and hence, these two features should be present in the power spectrum of flow coefficients, as well. First, we discuss that probably the most important concept for the universe, that of a causal horizon, very naturally applies to the case of relativistic heavy-ion collisions.

We noted above (Fig. 2) that initial state fluctuations of different length scales are present in relativistic heavy-ion collisions even for central collisions. The process of equilibration will lead to some level of smoothening. However, thermalization happens in a very short time scale. All estimates of the thermalization time τ_0 indicate very small values (as short as a tenth of fm for LHC energies). Hydrodynamical simulations can accommodate observed value of elliptic flow only with $\tau_0 < 1$ fm. No homogenization can be expected to occur beyond length scales larger than $c\tau_0$ at this thermaliza-

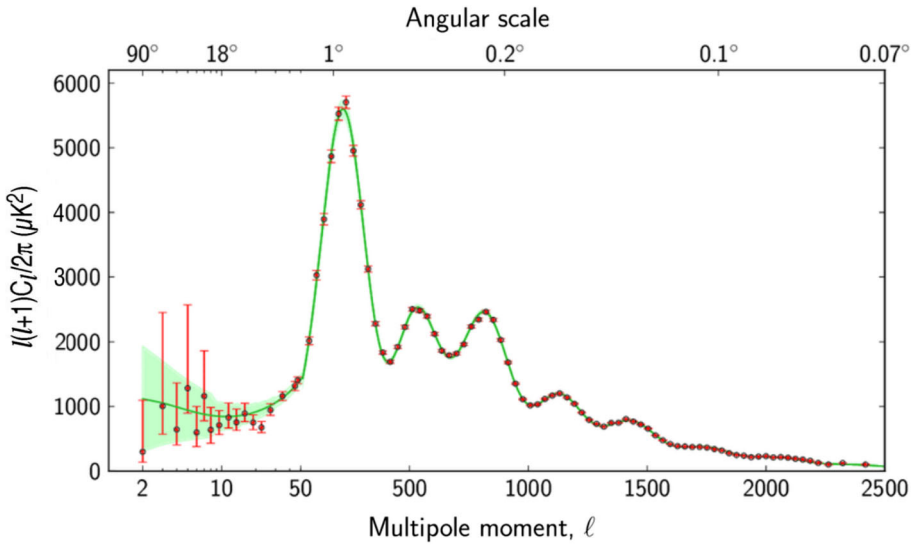

Fig. 3 CMBR power spectrum

tion stage. This provides a natural concept of causal Horizon. The interaction region resulting from the collision of the two highly Lorentz contracted nuclei is born at time $\tau = 0$ (definition of origin of time for full overlap of nuclei). It takes a time $\tau = \tau_0$ for this system to thermalize leading to a locally equilibrated system for which hydrodynamics becomes applicable. Relativistic hydrodynamics equations cannot lead to physical effects (of pressure differences etc.) being communicated beyond the causal distance $c\tau_0$. More precisely for the hydrodynamics, the limiting causal distance is the sound horizon $c_s\tau_0$ where c_s is the sound velocity ($= 1/\sqrt{3}$ for relativistic ideal plasma). Thus, inhomogeneities, especially anisotropies with wavelengths larger than this causal scale (horizon size), should be necessarily present at the thermalization stage when the hydrodynamic description is expected to become applicable. With the nucleon size being about 1.6 fm, the equilibrated matter will necessarily have density inhomogeneities with superhorizon wavelengths at the equilibration stage. As time increases, the horizon size increases with time and larger wavelength fluctuations become sub-horizon. The consequences of the presence of a sound horizon in the plasma in different higher harmonics were also discussed later in [53] where they also looked at the effect of viscosity on the dissipation of different scales.

We will now discuss coherence and acoustic oscillations in case of RHICE. Coherence of inflationary density fluctuations essentially results from the fact that the fluctuations initially are stretched to superhorizon sizes and are subsequently frozen out dynamically. In the context of heavy-ion collisions, this freezing out is similar to absence of initial transverse expansion velocity for QGP. Initially, fluctuations are only in spatial distribution of energy density, they become dynamical, converting to momentum anisotropies through hydrodynamical evolution. For all fluctuations of certain size λ, it happens ONLY after a certain time when horizon equals $\lambda/2$. Until then, the fluctuations are almost frozen. Thus, coherence (meaning phase locking [44]) will be expected to hold for RHICE also.

Let us now discuss the oscillatory behavior for the fluctuations. We simply note that small perturbations in a fluid will always propagate as acoustic waves, and hence, oscillations are naturally present. It may seem surprising, since typically, in the context of universe, the oscillations are discussed in the photon coupled baryonic system in the gravitational potential well of dark matter. This is indeed the main difference for RHICE from the universe, the absence of gravity for RHICE. However, in the universe, the only role of attractive gravity is to compress (collapse) the initial overdensities of cosmic fluid. Acoustic oscillations happen on top of these collapsed fluctuations simply, because the cosmic fluid is also governed by relativistic hydrodynamical equations (in expanding universe). Similar relativistic hydro equations govern fluid evolution for RHICE also (with Bjorken longitudinal expansion in the early stages). Thus, for RHICE, one will get harmonic oscillations (for a given mode) of plasma, while for the Universe, one gets oscillations of a forced oscillator (gravity acting as extra force) for the cosmic fluid. It can then be concluded that for RHICE also, there should be acoustic oscillations, which are coherent, just as for CMBR. It is important to realize that oscillations occur only for sub-horizon fluctuations. Only such fluctuations appear as perturbations in a background which can propagate as a sound wave; for superhorizon fluctuations, there is not enough time for pressure gradients to lead to oscillatory behavior.

The smaller the length scale of the fluctuation, the earlier it will enter the horizon and start oscillating till the freezeout occurs. Hence, the shortest scales will be most affected by any dissipative factors present in the system. In the absence of any damping, a plot of v_n^{rms} vs. n should have acoustic oscillation peaks similar to the CMBR power spectrum with the value of v_n^{rms} representing the stage of oscillation of the corresponding mode n at freezeout. The peak structure of v_n^{rms} vs. n plot shows which mode has undergone dominant

oscillations at the freezeout stage of the system. With time, various modes oscillate, depending on dissipation present in the system. Thus, the higher harmonics will provide information on the dissipative properties of the medium.

We now come to the second important feature of CMBR power spectrum: the behavior of modes which remain superhorizon at the surface of last scattering. We have seen above that these modes are suppressed in CMB. For heavy-ion collisions, behavior of such superhorizon fluctuations will be extremely important as these will carry information about long-range correlations in the initial state. These are large wavelength modes corresponding to low values of n in the plot of v_n^{rms}. We now argue that for RHICE as well, there is a similar (though not the same, due to absence of gravity here) importance of horizon entering of modes.

One can argue [15,16] that flow anisotropies for superhorizon fluctuations in heavy-ion collisions should be suppressed by a factor of order $H^s_{fr}/(\lambda/2)$ where H^s_{fr} is the sound horizon at the freezeout time τ_{fr} ($\sim$ 5–10 fm for typical Pb–Pb collision), and λ is the wavelength of fluctuation. This is because in heavy-ion collisions, spatial variations of density are not directly detected. This is in contrast to the Universe where the spatial density fluctuations are directly detected in terms of angular variations of CMBR temperature. For heavy-ion collisions, spatial fluctuation of a given scale (i.e., a definite mode) has to convert to fluid momentum anisotropy of the corresponding angular scale. This will get imprinted on the final hadrons and will be experimentally measured. This conversion of spatial anisotropy to momentum anisotropy (via pressure gradients) is not effective for superhorizon modes. Thus, superhorizon modes will be suppressed in heavy-ion collisions. It will be very important to understand suppression of low n harmonics as these will contain the information about freezeout horizon size as well as about long correlations at the initial stage.

We will see below that results from relativistic hydrodynamical simulations support this suppression of long-wavelength (low n) modes in the power spectrum of flow coefficients [54].

4 Study of higher flow coefficients

Extensive experimental effort has gone in determination of higher flow coefficients. The techniques typically require many-particle correlation methods as discussed above in Sect. 3. The first-ever plot for a large values of flow coefficients was presented by Sorensen in [32] and it was claimed that the plot shows suppression of superhorizon modes as predicted in [15,16]. Many experimental results have appeared since then. We show two sets of plots from ATLAS in Fig. 4 and ALICE in Fig. 5.

Figure 4 shows the plot of a large range of flow coefficients for Pb–Pb collision at 2.76 TeV at LHC. (ATLAS Preliminary, 2011, figure from arXiv: 1107.1468, Ref. [55]). Though it may be tempting to see some sort of acoustic peak like behavior in these plots for higher values of n, we note that errors in v_n are very large for $n \geq 6$ to reach any such conclusion. We thus focus on the plot for low values of n for which errors are in better control. The suppression of v_2 in the right plot is anomalous. This is exactly the behavior which was predicted in Ref. [15,16] where suppression of low n modes was termed as the *superhorizon suppression*. Suppression of v_1 is also important to note. Although, being the directed flow, it does not evolve as a sound mode governed by hydrodynamical evolution. It retains its initial value determined by initial state fluctuations, hence suppressed compared to higher modes which can grow due to hydrodynamical evolution.

Unfortunately, this suppression of v_n for low values of n is not seen in plots of v_n in Fig. 5 which shows recent data set from ALICE, 2020, showing plots of v_n for $n = 2-9$ for different centralities for Pb–Pb collision at $\sqrt{s_{NN}} = 5.02$ TeV. (Figure from arXiv: 2002.00633, Ref. [56]). While the data set of Fig. 5 is the latest data and is more refined, it may be noted that a direct comparison of Figs. 4 and 5 is difficult as the collision energies and centrality coverage are different for the two sets. Furthermore, note that v_1 is not shown in Fig. 5, while it is given in plots in Fig. 4. For the left plot in Fig. 4, it is the value of v_1 which shows the suppression. The right plot in Fig. 4 shows v_2 also to be suppressed (such a suppression of low n modes during hydrodynamical evolution was termed as the *superhorizon suppression* in Ref. [15,16]), while this is not seen in the plots in Fig. 5. It is important to emphasize here that the presence of first peak and its location, in the power spectrum, crucially depends on the freezeout time (size of acoustic horizon) and the wavelength of fluctuation being considered. Clearly, these will depend on the collision energy, as well as on centrality, along with the nature of initial state fluctuations.

At the same time, Fig. 5 shows something very important, which could not be clearly seen in Fig. 4 (due to large errors for v_n for large values of n in Fig. 4). Note the rise of v_n for $n > 7-8$ in Fig. 5 for all centralities except two cases (20–30% and 30–40%). Such a behavior is entirely unexpected from general considerations of flow coefficients. However, this is exactly the behavior expected from the presence of acoustic peaks in the power spectrum (similar to the CMBR case) as predicted in Refs. [15,16]). Errors for v_n for these larger values of n are in good control. This is the first clear indication of the presence of acoustic peaks in heavy-ion collisions.

We would like to conclude from Figs. 4 and 5 that the data show hints of non-trivial physics in the plots of v_n for a large values of n. Some of this has qualitative behavior of acoustic peaks in the power spectrum, and possibly even the presence of superhorizon suppression. Both these features need focused attention, as these can open a new direction to probe the early stages of the collision, in particular the spectrum of fluctuations and the medium properties. We now present results of hydrodynamics simulations [54] which show these two

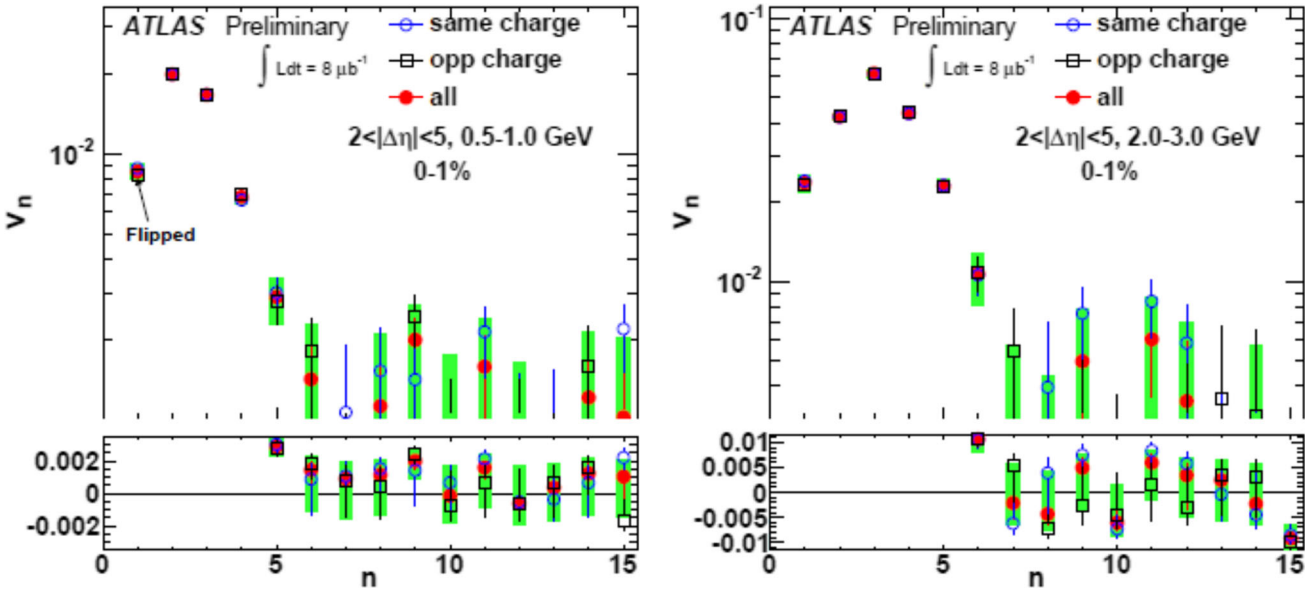

Fig. 4 Plot of a large range of flow coefficients for Pb–Pb collision at 2.76 TeV at LHC. ATLAS Preliminary, 2011. Note, errors in v_n become very large for $n \geq 6$. (Figure from arXiv: 1107.1468). We point out the anomalous suppression of v_2 in the right plot. Such a suppression of low n modes was predicted in Ref. [15,16] (termed as the *super-horizon suppression*). Suppression of v_1 is also important to note. Although, being the directed flow, it does not evolve as a sound mode governed by hydrodynamical evolution. It retains its initial value determined by initial state fluctuations, hence suppressed compared to higher modes which can grow due to hydrodynamical evolution

important features in the power spectrum of v_n, namely the acoustic peaks and suppression of power for low n mode (the superhorizon suppression).

We take QGP system in the ideal hydrodynamics limit with the energy momentum tensor of perfect fluid form:

$$T^{\mu\nu} = (\epsilon + P)u^\mu u^\nu + P\eta^{\mu\nu}, \tag{5}$$

where $\eta^{\mu\nu} = diag(-1, 1, 1, 1)$ is the Minkowski space–time metric, ϵ is the energy density, and P is the pressure. u^μ is the 4-velocity of the fluid.

Conservation of the energy-momentum tensor gives the equations for ideal relativistic hydrodynamics:

$$\partial_\mu T^{\mu\nu} = 0. \tag{6}$$

We take ideal gas equation of state in ultra-relativistic limit (with zero chemical potential so there is no baryon number conservation equation), $P = \epsilon/3$. We use a 3+1-dimensional code using leapfrog algorithm of second-order accuracy and QGP ideal gas equation of state for two massless flavors. The initial conditions here are provided in terms of a Wood–Saxon background plus randomly placed Gaussian fluctuations of specific widths. We use these initial conditions as it allowed for control on the size of initial fluctuations, so that its effects on the locations of acoustic peaks could be directly studied. We calculate the Fourier coefficients for the spatial anisotropies of the energy density (by calculating net energy contained in a given angular bin) at the initial stage, and then using hydrodynamical evolution, calculate the Fourier coefficients of the resulting momentum anisotropy in $\Delta p/p$ in different angular bins at a later stage. As we mentioned above, we use a fixed lab frame, and calculate respective power spectra (of spatial anisotropies and momentum anisotropies, respectively) using root-mean-square values of the respective Fourier coefficients. For details of the simulations, we refer to Ref. [54].

Figure 6 shows plots of these power spectra from the simulation for a central collision. Dotted curve with solid dots shows the plot of initial power spectrum of spatial anisotropies. Dashed curve with stars shows the power spectrum of resulting momentum anisotropies (at proper time $\tau = 1.98$ fm, we could not evolve the system for large times due to certain instabilities for large fluid velocities, see [54] for a discussion). Comparison of the two plots shows important qualitative difference for low n. We note that for n larger than about 4, both plots show roughly similar pattern. However for smaller n, the two plots show dramatic difference. Plot for spatial anisotropies keeps rising monotonically with decreasing n. However, plot for momentum anisotropies (resulting from the spatial anisotropies) shows a drop for low n values. This suppression of *super-horizon modes* was predicted in Ref. [15,16] resulting from the fact that these large wavelength modes do not get enough time to transfer to momentum anisotropies. As we discussed above, hints for this suppression for low n values are seen in the experimental plots in Fig. 4, though latest data shown in Fig. 5 do not seem to support it. There is a hint of a second peak in Fig. 6 in the power spectrum of momentum anisotropies near $n \sim 8 - 9$. As we mentioned above, these results are for short time scale, $\tau = 1.98$ fm. One would not

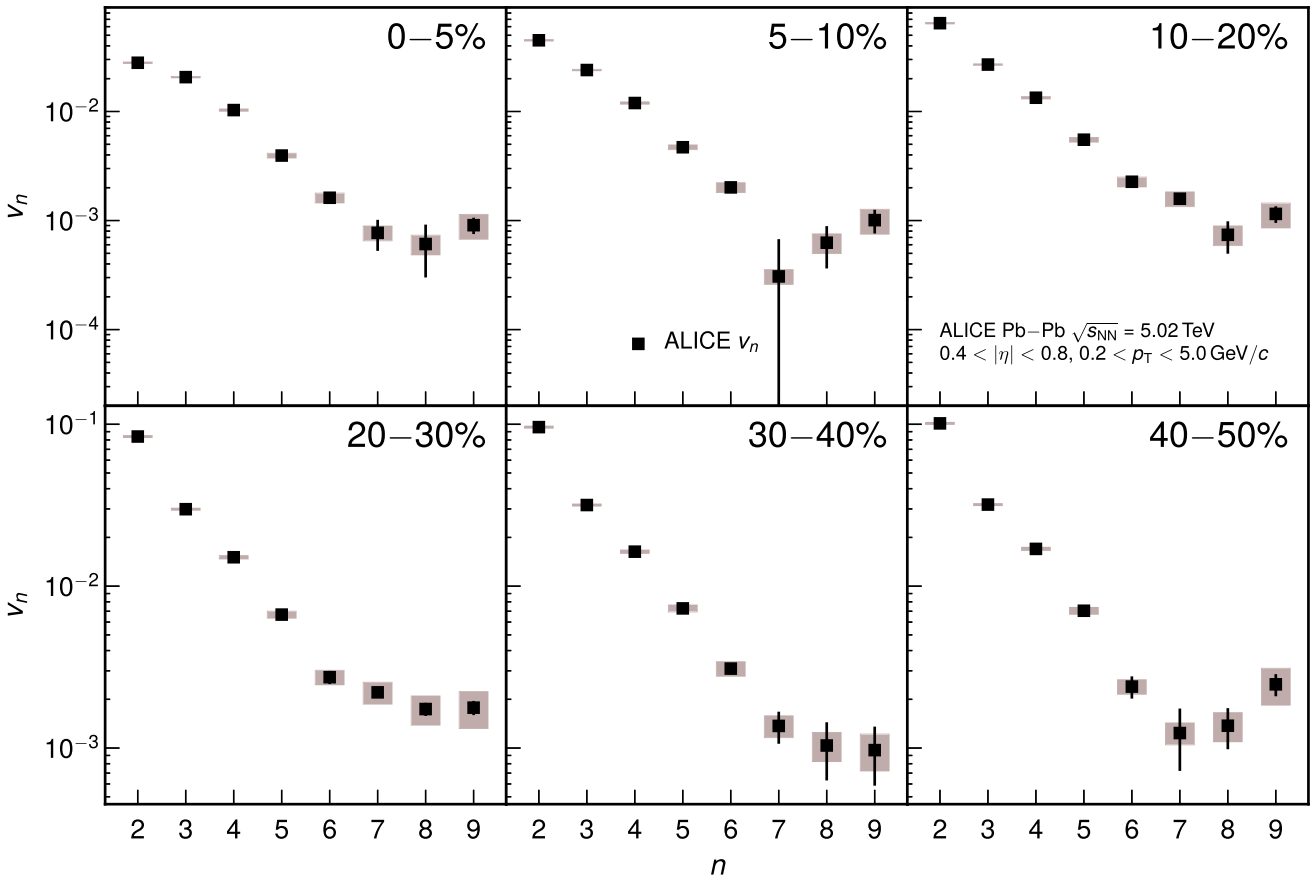

Fig. 5 Recent data set from ALICE (2020), showing plots of v_n for $n = 2-9$ for different centralities for Pb–Pb collision at $\sqrt{s_{NN}} = 5.02$ TeV. (Figure from arXiv: 2002.00633). Note that the anomalous suppression of v_2 in the right plot in Fig. 4 (the *superhorizon suppression* [15,16]), is not seen in the plots in Fig. 5. Also note that value of v_1 in Fig. 4 also shows suppression, while v_1 is not shown in Fig. 5. (Note the comments about v_1 suppression in Fig. 4). For the comparison of Figs. 4 and 5, we point out that, while Fig. 5 shows the latest data which is more refined, a direct comparison of Figs. 4 and 5 is difficult as the collision energies and centrality coverage are different for the two sets. As discussed in the text, physics of acoustic peaks can crucially depend on these. Most important feature for plots in Fig. 5 is the rise of v_n for $n > 7-8$. This rise will be entirely unexpected from general considerations of flow coefficients, while this is exactly the behavior expected from the presence of acoustic peaks in the power spectrum (similar to the CMBR case) as predicted in refs. [15,16])

expect full development of any acoustic peaks in such a short time interval. Clearly further efforts are needed to probe these very important features. If these are indeed found to be present, then suppression of this momentum anisotropy for low n values (compared to spatial anisotropies), along with possible existence of a second acoustic peak, will be very surprising, indicative of a rich physics of existence of causal (sound) horizon, suppression of superhorizon modes, as well as acoustic oscillations in relativistic heavy-ion collisions.

5 Initial magnetic field and flow coefficients

As our focus has been to investigate initial state fluctuations, it is important to know how to separate them from the effects of hydro evolution. What one needs to use is some technique which can, in some way, isolate the quantitative values of fluctuations at very early stages. We discuss below how to achieve it with the effects of magnetic field on the power spectrum of flow.

There has been a tremendous interest in the effects of initial magnetic field on the evolution of system in relativistic heavy-ion collisions. In non-central collisions, at the center of system, the magnetic field produced by motion of nuclei is perpendicular to the *reaction plane* (plane formed by the impact parameter vector and the line of motion of nuclei, xz-plane in our case). It is known that one can get extremely large magnetic field in these experiments, having strength of the order of $10^{14} - 10^{15}$ Tesla (at the center of system), beyond the values anywhere else in the observed universe. Some of the main motivations of these studies have been to use this magnetic field to directly probe highly non-perturbative physics of QCD such as effects of instantons; also the effects of sphaleron at a very high temperature and in the out-of-equilibrium state arising from

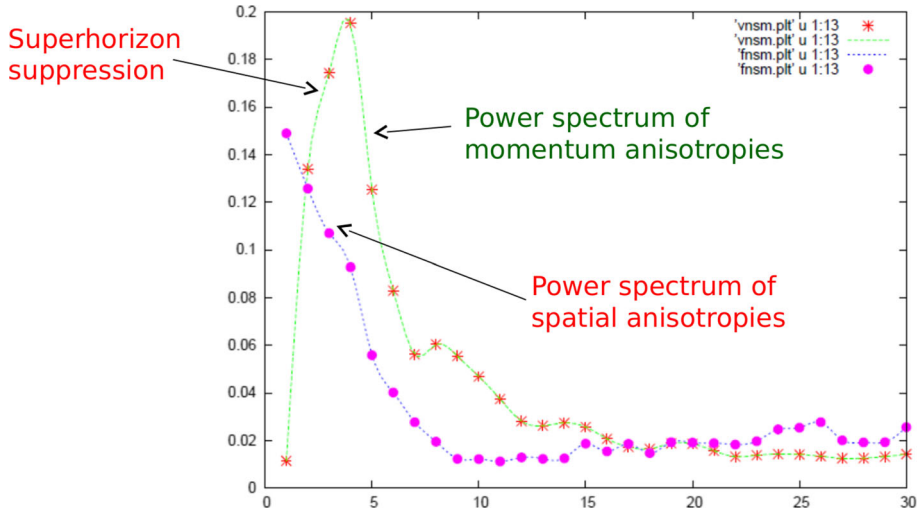

Fig. 6 Suppression of low n modes. Note that the power in low n modes for spatial anisotropies monotonically increases with decreasing n (for central collision). However, while hydro evolution converts these shape anisotropies to momentum anisotropies in a proportional manner for high values of n, it is completely reverse behavior for low values of n. This is exactly what is expected of superhorizon modes for which the hydro equations do not have enough time to convert the spatial anisotropy to momentum anisotropy in a proportional manner (not necessarily assuming the same proportional factor for all n). We also point out hints of second peak in the power spectrum of momentum anisotropies near $n \sim 8-9$. As these results are for short time scale $\tau = 1.98$ fm, one would not expect full development of any acoustic peaks

the so-called chiral magnetic effect [57]. These processes create the domains of gluonic configuration having non-zero integral topological charge, typically either + 1 or − 1. In such domains, a chirality imbalance is created due to the *chiral anomaly* of QCD, i.e., depending upon the topological charge of the configuration, either right-handed chirality dominates or left handed (working in the *chiral limit*). On the other hand, a strong magnetic field aligns the spin magnetic moment of particles along its direction; spin of positive charge particles is aligned along the direction of magnetic field and spin of negative charge particles in the opposite direction. In the domains of non-zero topological charge, depending upon the chirality dominance, this leads the opposite motion of positive and negative charge particles, and a local electric current is generated perpendicular to the reaction plane. In general, there will be many such domains having different chirality imbalance, which will therefore have opposite directions of this local current. However, since the formation of these domains is lead by statistical process, there can be an overall non-zero topological charge due to spacetime fluctuations of such topologically non-trivial gluonic configurations, which can lead an overall electric charge separation and generate electric current perpendicular to the *reaction plane*. This is known as the *chiral magnetic effect* (CME) [57], which is being extensively investigated, see review [58]. One of the main problems in this regard is that the magnetic field is strong only at very early times, decaying by few orders of magnitude within a fm time. It was pointed out by Tuchin [59,60] that since the plasma forms within less than a fm/c time, the rapidly decreasing magnetic field will induce circular currents in the medium, and as a result, the induced magnetic field will survive for much longer times, the relaxation time depending on the conductivity of the plasma. But even with the medium effects, the extremely large initial values of magnetic field do not last for any significant time period. Therefore, chiral magnetic effect is expected to dominantly occur in the pre-equilibrium stage of the collision. It has also been argued that the effects of conductivity do not play an important role for realistic values, and the medium effects are much more suppressed [61] (see, also [62] in this context).

While this becomes a limitation for studying chiral magnetic effect etc., we suggest that this limitation can be used to our benefit in isolating the initial distribution of fluctuations from their later evolution. Magnetic field, present at the thermalization time, can affect the whole evolution of the fluid. It can affect the elliptic flow, and in general affects all flow coefficients; the entire power spectrum of flow coefficients can be affected by the magnetic field. Interestingly, this is exactly what happens for CMBR power spectrum also [63]. Indeed, that was the motivation for some of us to initiate the study of effects of initial magnetic field on flow coefficients, in particular on the elliptic flow in relativistic heavy-ion collisions, see ref. [64].

We briefly recall the discussion of effect of magnetic field on elliptic flow v_2 from ref. [64], where it was pointed out that an initial magnetic field can enhance elliptic flow; a similar enhancement was also confirmed in an analysis by Tuchin [65]. The basic physics argument in Ref. [64] is as follows. Consider a non-central collision, as shown in Fig. 1. The moving spectators lead to generation of magnetic field B_0 along y-axis (with

impact parameter vector being along x-axis) in the central region. When a thermalized medium forms, this magnetic field remains present, even though with relatively smaller strength, and may get trapped inside the plasma. In the presence of magnetic field, there are different types of waves in the plasma. There are fast magnetosonic waves which are generalized sound waves with significant contributions from the magnetic pressure. These waves have speed $\sqrt{c_s^2+v_A^2}$, where $c_s{=}\sqrt{\frac{\partial p_g}{\partial \epsilon}}$ is the hydrodynamics sound speed, $v_A{=}\frac{B_0}{\sqrt{4\pi\epsilon}}$ is the Alfvén speed, p_g is the thermal pressure, and ϵ is the energy density of the plasma. The increment in the speed of such sound waves arises, basically because under the expansion, distortions of magnetic field lines along the x-direction cost energy, because of which the equation of state becomes stiffer in this direction, causing increment in the sound speed. In the y-direction, the sound speed remains unchanged, i.e., remains equal to c_s. It can be seen that with the development of flow from a pressure gradient (using Euler's equations [66,67]), the resulting flow velocity is proportional to sound speed square. As the sound velocity becomes larger in the x-direction, it follows that flow in this direction will be enhanced, while in the y-direction, it will not change. This can lead to the enhancement of the elliptic flow v_2.

However, the physics of this effect is not that simple, as other factors can be present. For example, under certain situations, specially in the high impact parameter regime of collisions, extent of magnetic field lies beyond the plasma region along the x-direction. In that case, the expansion of a conducting plasma into regions of magnetic field gets hindered. One can expect it from Lenz's law: expanding conductor squeezes magnetic flux, which opposes expansion of the plasma. Such an argument will imply suppression of v_2 due to magnetic field. However, as discussed in Ref. [64], distortions of magnetic field lines try to enhance the flow along x-direction. In general, all such factors will be present affecting the flow in a complex manner. As we will see below, depending on the situation, specifically, extent of the plasma region in comparison to the extent of region of strong magnetic field, one of these factors may dominate over the other. Along with these, fluctuations also play important role and the final effect is a combination of all these.

The quark-gluon plasma, produced in relativistic heavy-ion collisions, has a finite electric conductivity which varies spatially as well as temporally. However, for simplicity, we take the ideal magneto-hydrodynamic approximation for this fluid, in which the electric conductivity is considered infinite at each spacetime point. The ideal relativistic magneto-hydrodynamics (RMHD) equations are [68]:

(a) The baryon number conservation equation:

$$\partial_\alpha(nu^\alpha)=0. \tag{7}$$

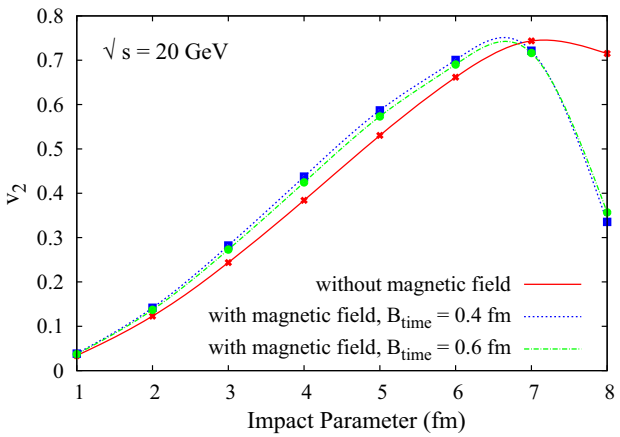

Fig. 7 Effect of initial magnetic field on the elliptic flow [69]

(b) The energy–momentum conservation equations:

$$\partial_\alpha\Big((\epsilon+p_g+|b|^2)u^\alpha u^\beta-b^\alpha b^\beta+\big(p_g+\frac{|b|^2}{2}\big)\eta^{\alpha\beta}\Big)=0. \tag{8}$$

(c) The homogeneous Maxwell's equations:

$$\partial_\alpha(u^\alpha b^\beta-u^\beta b^\alpha)=0. \tag{9}$$

Here, n, ϵ, and p_g are baryon number density, energy density, and thermal pressure, respectively. $u^\alpha=\gamma(1,\mathbf{v})$ is the four-velocity of the fluid. The Minkowski metric is $\eta_{\alpha\beta}=diag(-1,1,1,1)$, the four-vector $b^\alpha=\gamma\Big(\mathbf{v}.\mathbf{B},\frac{\mathbf{B}}{\gamma^2}+\mathbf{v}(\mathbf{v}.\mathbf{B})\Big)$, and $|b|^2{=}b^\alpha b_\alpha$. Therefore, the total pressure of the fluid is $p=p_g+\frac{|\mathbf{B}|^2}{2\gamma^2}+\frac{(\mathbf{v}.\mathbf{B})^2}{2}$. By following formalism from Ref. [68] to solve these equations, we carry out ideal relativistic magneto-hydrodynamic simulations for evolution of QGP produced in relativistic heavy-ion collisions. We take an initial profile of magnetic field for given impact parameter of the collision at the thermalization time of the system, calculated by taking electric field for uniformly charged nuclei, and Lorentz transforming it for their opposite motion. We carry out (3+1)-dimensional simulation using Glauber-like initial energy density for QGP, with profile along z-direction being Woods–Saxon with appropriate parameters. We show our simulation result of effect of magnetic field on the elliptic flow in Fig. 7, see Ref. [69].

We see that magnetic field enhances v_2 for small impact parameters. However, with increasing impact parameter, the enhancement increases first and then decreases. Eventually, at very large impact parameters, magnetic field suppresses the elliptic flow. This non-trivial effect of magnetic field on v_2 arises due to the following reasons. If magnetic field is almost entirely

contained within the plasma region, elliptic flow gets enhanced by the magnetic field. This is only possible for small values of the impact parameter. This is in accordance with the argument of having a stiffer equation of state along x-direction due to the magnetic field along y-direction. However, if the magnetic field extends well beyond the plasma region along x-direction, then elliptic flow is suppressed by the magnetic field due to the Lenz's law. This situation arises when impact parameter is large.

Refs. [70,71] also study the effects of magnetic field on elliptic flow by performing ideal RMHD simulations. In [71], it is shown that a strong magnetic field can enhance elliptic flow, where the magnetic field generated by electric current arising due to CME (I_{cme}) in the pre-equilibrium stage also has been considered along with the classical origin of magnetic field. The classical origin of magnetic field is calculated in a medium with a non-zero electric conductivity. The total magnetic field profile arising from these two sources is set as the initial condition for the evolution of the fluid. The parameter which enters for the calculation of magnetic field of CME origin is the *chiral magnetic conductivity* σ_χ [72], which is a proportionality constant of $I_{cme} \propto \mathbf{B}$. It is found that the magnetic field generated due to the CME has opposite effects on the elliptic flow, i.e., it has tendency to suppress the elliptic flow even in low impact parameter regime [71]. In that work, the dependence of electric conductivity and σ_χ on the initial magnetic field profile and its effect on elliptic flow has also been studied. In ref. [73] by performing reduced-magnetohydrodynamical simulations for expansion of hot and dense nuclear matter in (2+1)-dimensions, the enhancement of v_2 is reported. In Ref. [74] also, effect of an inhomogeneous magnetic field on the transverse flow has been investigated.

In our simulation [69], we also find that fluctuations in the initial energy density can lead to temporary increase of magnetic field in some fluid regions due to flux-rearrangement by evolving initial state density fluctuations, which can push flux lines, leading to temporary and localized concentration of flux lines. This will be important for CME which is sensitive to locally strong magnetic field (instanton size regions).

We now show an important qualitative effect of magnetic field on the power spectrum of flow coefficients. Figure 8 shows the power spectrum of flow for magnetic field with strength $5m_\pi^2$ [69]. As this plot is for a strong magnetic field, simulation could be carried out only for short time of 0.6 fm. We see a pattern of different powers in even and odd $v_n^{\rm rms}$ coefficients at low n. This is expected from the reflection symmetry about the magnetic field direction if initial state fluctuations are not dominant. This is a qualitatively distinct result with unambiguous signal for the presence of strong magnetic field during early stages.

Note that the even-odd pattern is seen in Fig. 8 for only first few flow coefficients as fluctuation effects wash out the effect for larger v_n^{rms} for the event average over 10 events. As fluctuations are necessarily present at the initial stage itself, this signal will be in general suppressed in the final flow power spectrum. This could be one possible reasons why there is no hint of such features in the data in Figs. 4 and 5. Of course, it is also possible that strong enough magnetic field may not last for significant time for this feature to develop sufficiently. To illustrate the effect of initial fluctuations on this feature, we show in Fig. 9 flow fluctuations for a smooth isotropic plasma region (without any fluctuations) in the presence of magnetic field. We now take a more reasonable value of magnetic field strength equal to m_π^2. Due to smaller magnetic field and smooth plasma profile, the evolution could be run up to 3 fm time (after which boundary effects could not be neglected). We see a strong even–odd power difference in the power spectrum even for large n values.

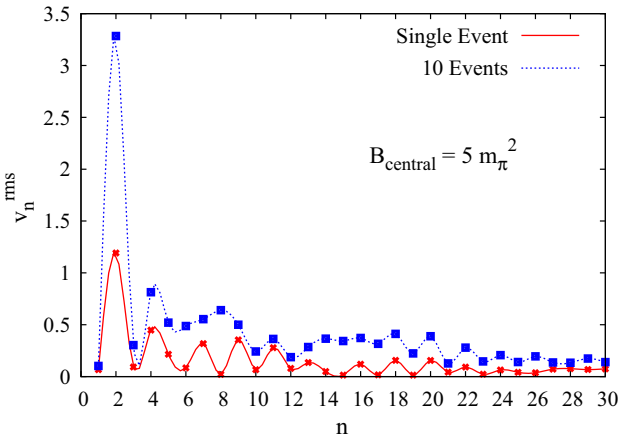

Fig. 8 Plot of v_n^{rms} for magnetic field with strength $5m_\pi^2$. Even-odd power difference is seen in first few flow coefficients as fluctuations wash out the effect for large v_ns [69]. There is no hint of such features in the data in Figs. 4, 5 which could be due to strong initial fluctuations, or simply that strong enough magnetic field does not survive for any significant time

The suppression of this qualitative even-odd signal for flow power spectrum (e.g., absence of such a feature in Figs. 4, 5) provides us an independent probe of initial state fluctuations. As the magnetic field is strong only for very early stages, the evolution of flow power spectrum during those stages will be a result of complex interplay of magnetic field effect, producing even-odd power differences, and existence of fluctuations, which tend to suppress these qualitative features. A comparison with detailed simulations should be able to shed some light on the nature of fluctuations during very early stages when the magnetic field was strong.

Now, we discuss very briefly another aspect of QCD matter which may affect v_2. An ideal MHD fluid has a property of diamagnetism, which opposes any change in the strength of magnetic field if fluid is at rest; magnetic flux lines are conserved in this fluid. As we mentioned earlier, in this fluid, an additional momentum anisotropy arises due to larger sound speed along x-direction. In contrary to this, it is shown in Ref. [75] that the QCD medium has a property of paramag-

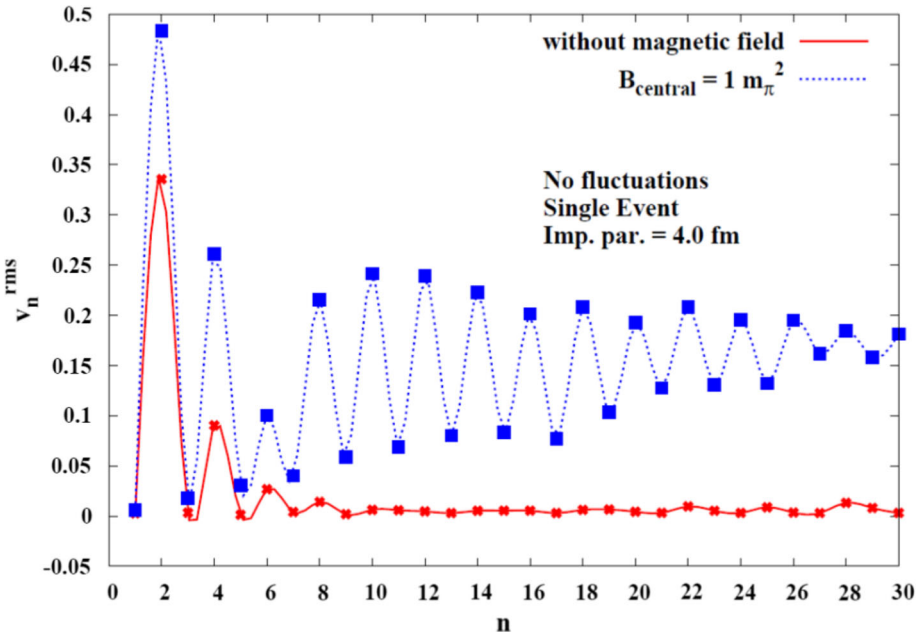

Fig. 9 Plot of v_n^{rms} for magnetic field with strength m_π^2. Here, we consider isotropic region with smooth plasma profile without any fluctuations. Strong difference in the power of even and odd values of v_n^{rms} are present arising from the effect of magnetic field [69]

netism, which supports changes in the strength of magnetic field. It is then argued that this feature may create an additional spatial anisotropy in the fluid simply, because such fluid will move toward the region of stronger magnetic field, which may make plasma more squeezed along x-direction [75]. This process is named as *paramagnetic squeezing*. This additional spatial anisotropy may affect v_2 depending upon the impact parameter of the collisions [75]. Note that in Ref. [76], suppression in v_2 due to this effect has been reported. However, in that work, a magnetic field profile with non-zero divergence was used, so results may not be conclusive.

5.1 Flow anisotropies and superfluid phases of QCD

It turns out that this qualitative behavior of even–odd power difference for flow coefficients can also arise from an entirely different source. If there are superfluid vortices present during early stages of low-energy heavy-ion collisions, they can also lead to such features [2]. Of course, in that case, there will be additional signals, such as a very strong elliptic flow even in the central collisions, negative elliptic flow for some specific configuration of vortices in non-central collisions, etc. [2], which can be used to differentiate from the effect of magnetic field sourced even-odd power difference. There is a remarkable variety of exotic phases of QCD at very large baryon density, e.g., color flavor locked (CFL) phase, 2SC phase, crystalline superconductivity, etc. These are color superconducting phases of QCD arising from di-quark condensates, with quarks near the Fermi surface forming Cooper pairs at very high baryon density [1]. Some of these phases, e.g., CFL phase, lead to superfluidity. Interestingly, even at relatively low baryon densities, the nucleonic superfluidity with neutrons forming Cooper pairs (for protons, one gets superconductivity) also exists, which is typically found in the interiors of neutron stars.

Such superfluid phases may become accessible in relatively low-energy heavy-ion collisions, e.g., at FAIR and NICA, and possibly at the beam energy scan program of RHIC. Any transition to superfluid phase will invariably lead to formation of superfluid vortices whose initial number density can be estimated from reasonably model independent topological arguments (see, [2]). It is clear that any superfluid vortex at the initial stage will dramatically affect the resulting flow pattern. This was investigated in Ref. [2] using relativistic hydro simulations, incorporating initial vortex configurations and several qualitatively new features were found. For example, a strong even–odd power difference in the power spectrum of flow coefficients was found, similar to shown in Figs. 8, 9. Along with that, strong elliptic flow in central collisions and negative elliptic flow in non-central collisions were also found, where different possibilities arise for different initial vortex configurations. Thus, with these, one can distinguish the source of any even–odd power difference from the effect of initial magnetic field. More importantly, the two effects arise in entirely different regimes of QCD phase diagram. Strong magnetic field only occurs at ultra-relativistic collisions, e.g., at highest energies of LHC which invariably has very small baryonic chemical potential associated with the produced QGP. Therefore, there is no possibility of any superfluid QCD phases arising in that energy regime. On the other hand, low-energy collisions at FAIR, NICA, BES program of RHIC, which may have a high value of baryon chemical potential are not expected to have very high magnetic fields which could lead to any significant even–odd effect for the flow power spectrum.

6 Conclusions and future directions

We have provided a short review of a very specific topic, focusing on the power spectrum of flow fluctuations in relativistic heavy-ion collisions. The thermalized medium formed from collision of two heavy nuclei is viewed exactly in the same manner as the initial matter-energy density in the universe with associated density fluctuations. These density fluctuations get imprinted into the final particle momentum distributions, just as for the universe, the initial primordial density fluctuations manifest in final photon distributions leading to CMBR power spectrum. With that lesson in mind from the universe, the power spectrum of flow fluctuations becomes an excellent probe for the initial state fluctuations in heavy-ion collisions. The physics underlying the evolution of initial density fluctuations is very similar in both cases, simply governed by relativistic hydrodynamical equations in expanding plasma (though expansions are different in both cases). The only important difference between the two cases being absence of gravity for RHICE. However, it is easy to see that the presence of acoustic peaks is independent of the presence of gravity, simply resulting from sound modes in a plasma and the superhorizon density fluctuations are necessarily present in RHICE at the initial stage. One of the most important features expected in the power spectrum of flow coefficients is the suppression of long-wavelength modes or the low n flow coefficients. There seems clear experimental evidence for the suppression of long-wavelength fluctuations (lower n flow coefficients) in experimental data and it is important to focus on these to probe long-range correlations at initial stage. This will shed light on the presence of long-scale correlations in initial parton distributions (which will be probed by the upcoming electron-ion collider), and also on the size of sound horizon at the freezeout stage (just like for CMBR, the first peak signals the size of causal horizon at the surface of last scattering). We have also discussed how the existence of strong magnetic field in very early stages of plasma evolution (which rapidly decays, even with medium effects) can be used to isolate the initial values of density fluctuations from the effects of their subsequent evolution. This is in terms of a qualitative effect of strong magnetic field leading to difference in power of even–odd flow coefficients. As initial fluctuations suppress these effects, therefore with proper numerical simulations, one may be able to use the suppression of these qualitative feature to provide us an independent probe of initial state fluctuations.

Acknowledgements We acknowledge useful discussions with Sanatan Digal, Minati Biswal, and Abhishek Atreya.

Funded by SCOAP[3].

References

1. M.G. Alford, A. Schmitt, K. Rajagopal, T. Schafer, Rev. Mod. Phys. **80**, 1455 (2008)
2. Arpan Das, Shreyansh S. Dave, Somnath De, Ajit M. Srivastava, Mod. Phys. Lett. A **32**, 1750170 (2017)
3. J.-Y. Ollitrault, Phys. Rev. D **46**, 229 (1992)
4. P.F. Kolb, P. Huovinen, U. Heinz, H. Heiselberg, Phys. Lett. B **500**, 232 (2001)
5. R. A. Lacey, A. Taranenko, arXiv:nucl-ex/0610029
6. N. Borghini, J.-Y. Ollitrault, Phys. Lett. B **642**, 227 (2006)
7. P. Kovtun, D.T. Son, A.O. Starinets, Phys. Rev. Lett. **94**, 111601 (2005)
8. J. Adams et al. (STAR Collaboration), Phys. Rev. **C 72**, 014904 (2005), S. S. Adler al. (PHENIX Collaboration), Phys. Rev. Lett. **91**, 182301 (2003)
9. C. Alt et al., NA49 Collaboration. Phys. Rev. C **68**, 034903 (2003)
10. P. Sorensen (for the STAR collaboration), J. Phys. **G 34**, S897 (2007)
11. S. Manly et al. (for PHOBOS collaboration), arXiv:nucl-ex/0702029
12. R. S. Hollis et al. (for PHOBOS collaboration), arXiv:nucl-ex/0707.0125
13. H. Sorge, Phys. Rev. Lett. **82**, 2048 (1999)
14. R. Snellings, arXiv: 1102.3010
15. A.P. Mishra, R.K. Mohapatra, P.S. Saumia, A.M. Srivastava, Phys. Rev. C **77**, 064902 (2008)
16. A.P. Mishra, R.K. Mohapatra, P.S. Saumia, A.M. Srivastava, Phys. Rev. C **81**, 034903 (2010)
17. S. Voloshin, Y. Zhang, Z. Phys. C **70**, 665 (1996) https://doi.org/10.1007/s002880050141[hep-ph/9407282]
18. J. Barrete et al., Phys. Rev. C **55**, 1420 (1997)
19. A.M. Poskanzer, S.A. Voloshin, Phys. Rev. C **58**, 1671 (1998)
20. S.A. Voloshin, A.M. Poskanzer, A. Tang, G. Wang, Phys. Lett. B **659**, 537 (2008)
21. S. Wang et al., Phys. Rev. C **44**, 1091 (1991). https://doi.org/10.1103/PhysRevC.44.1091
22. N. Borghini, P. M. Dinh, J. Y. Ollitrault, Phys. Rev. C **64**, 054901 (2001) https://doi.org/10.1103/PhysRevC.64.054901[nucl-th/0105040]
23. R. S. Bhalerao, J. Y. Ollitrault, Phys. Lett. B **641**, 260 (2006) https://doi.org/10.1016/j.physletb.2006.08.055[nucl-th/0607009]
24. J.Y. Ollitrault, A.M. Poskanzer, S.A. Voloshin, Phys. Rev. C **80**, 014904 (2009). https://doi.org/10.1103/PhysRevC.80.014904 ([arXiv:0904.2315 [nucl-ex]].)

25. J.P. Blaizot, in the International Conference on *Matter at extreme conditions: Then and Now*, held at Bose Inst., Kolkata, India, Jan. 15-17 (2014)
26. A. Mocsy, P. Sorensen, arXiv:1008.3381 [hep-ph]
27. P. Sorensen, J. Phys. G **37**, 094011 (2010). https://doi.org/10.1088/0954-3899/37/9/094011 ([arXiv:1002.4878 [nucl-ex]].)
28. B. Alver, G. Roland, Phys. Rev. C **81**, 054905 (2010) Erratum: [Phys. Rev. C **82**, 039903 (2010)] https://doi.org/10.1103/PhysRevC.82.039903, https://doi.org/10.1103/PhysRevC.81.054905 [arXiv:1003.0194 [nucl-th]]
29. C. Gale, S. Jeon, B. Schenke, P. Tribedy, R. Venugopalan, Nucl. Phys. A **904905**, 409c (2013)
30. G.Y. Qin, H. Petersen, S.A. Bass, B. Muller, Phys. Rev. C **82**, 064903 (2010). https://doi.org/10.1103/PhysRevC.82.064903 ([arXiv:1009.1847 [nucl-th]].)
31. U. Heinz, R. Snellings, arXiv: 1301.2826
32. P. Sorensen, arXiv:0808.0503
33. A. Mocsy, P. Sorensen, Nucl. Phys. A **855**, 241 (2011)
34. J.I. Kapusta, Nucl. Phys. A **862–863**, 47 (2011)
35. J.Y. Ollitrault, J. Phys. Conf. Ser. **312**, 012002 (2011)
36. K. Aamodt *et al.* [ALICE Collaboration], Phys. Rev. Lett. **107**, 032301 (2011) https://doi.org/10.1103/PhysRevLett.107.032301[arXiv:1105.3865 [nucl-ex]]
37. A. Adare *et al.* [PHENIX Collaboration], Phys. Rev. Lett. **107**, 252301 (2011) https://doi.org/10.1103/PhysRevLett.107.252301[arXiv:1105.3928 [nucl-ex]]
38. G. Aad *et al.* [ATLAS Collaboration], JHEP **1311**, 183 (2013) https://doi.org/10.1007/JHEP11(2013)183[arXiv:1305.2942 [hep-ex]]
39. R.A. Lacey, R. Wei, N.N. Ajitanand, A. Taranenko, Phys. Rev. C **83**, 044902 (2011). https://doi.org/10.1103/PhysRevC.83.044902 ([arXiv:1009.5230 [nucl-ex]].)
40. R.S. Bhalerao, M. Luzum, J.Y. Ollitrault, Phys. Rev. C **84**, 034910 (2011). https://doi.org/10.1103/PhysRevC.84.034910 ([arXiv:1104.4740 [nucl-th]].)
41. J. Qian, U. W. Heinz, J. Liu, Phys. Rev. C **93**, no. 6, 064901 (2016) https://doi.org/10.1103/PhysRevC.93.064901[arXiv:1602.02813 [nucl-th]]
42. L. V. Bravina *et al.*, Eur. Phys. J. C **74**, no. 3, 2807 (2014) https://doi.org/10.1140/epjc/s10052-014-2807-5[arXiv:1311.7054 [nucl-th]]
43. A. M. Sirunyan *et al.* [CMS Collaboration], arXiv:1910.08789 [hep-ex]
44. S. Dodelson, *Modern cosmology* (Academic Press, California, 2003)
45. T.A. Trainor, D.T. Kettler, Int. J. Mod. Phys. E **17**, 1219 (2008). https://doi.org/10.1142/S0218301308010465 ([arXiv:0704.1674 [hep-ph]].)
46. P. Naselsky et al., Phys. Rev. C **86**, 024916 (2012). https://doi.org/10.1103/PhysRevC.86.024916 ([arXiv:1204.0387 [hep-ph]].)
47. G. Sarwar, J. e. Alam, Int. J. Mod. Phys. A **33**, no. 08, 1850040 (2018) https://doi.org/10.1142/S0217751X18500409[arXiv:1503.06019 [nucl-th]]
48. F. J. Llanes-Estrada, J. L. Muoz Martinez, Nucl. Phys. A **970**, 107 (2018) https://doi.org/10.1016/j.nuclphysa.2017.11.005[arXiv:1612.05036 [hep-ph]]
49. G. Sarwar, S. K. Singh, J. e. Alam, Int. J. Mod. Phys. A **33**, no. 20, 1850121 (2018) https://doi.org/10.1142/S0217751X1850121X[arXiv:1711.03743 [nucl-th]]
50. M. Machado, P. H. Damgaard, J. J. Gaardhje, C. Bourjau, Phys. Rev. C **99**, no. 5, 054910 (2019) https://doi.org/10.1103/PhysRevC.99.054910[arXiv:1812.07449 [hep-ph]]
51. M. Machado, arXiv:1907.00413 [hep-ph]
52. S. Basu, R. Chatterjee, B.K. Nandi, T.K. Nayak, AIP Conference Proceedings **1701**, 060004 (2016). (arXiv:1405.3969)
53. P. Staig, E. Shuryak, Phys. Rev. C **84**, 034908 (2011), see also, *ibid* Phys. Rev. **C84**, 044912 (2011)
54. P.S. Saumia, A.M. Srivastava, Mod. Phys. Lett. A **31**, 1650197 (2016)
55. J. Jia for the ATLAS Collaboration, arXiv: 1107.1468
56. ALICE Collaboration, arXiv: 2002.00633
57. D.E. Kharzeev, L.D. McLerran, H.J. Warringa, Nucl. Phys. A **803**, 227 (2008)
58. Jie Zhao, IJMP A **33**, 1830010 (2018)
59. K. Tuchin, Phys. Rev. C **83**, 017901 (2011)
60. K. Tuchin, Phys. Rev. C **82**, 034904 (2010)
61. L. McLerran, V. Skokov, Nucl. Phys. A **929**, 184 (2014)
62. E. Stewart, K. Tuchin, Phys. Rev. C **97**, 044906 (2018)
63. J. Adams, U.H. Danielsson, D. Grasso, H. Rubinstein, Phys. Lett. B **388**, 253 (1996)
64. R.K. Mohapatra, P.S. Saumia, A.M. Srivastava, Mod. Phys. Lett. A **26**, 2477 (2011)
65. K. Tuchin, J. Phys. G **39**, 025010 (2012)
66. J.-Y. Ollitrault, Eur. J. Phys. **29**, 275 (2008)
67. R.S. Bhalerao, J.P. Blaizot, N. Borghini, J.-Y. Ollitrault, Phys. Lett. B **627**, 49 (2005)
68. A. Mignone, G. Bodo, Mon. Not. R. Astron. Soc. **368**, 1040 (2006)
69. Arpan Das, Shreyansh S. Dave, Saumia P.S., Ajit M. Srivastava, PRC **96**, 034902 (2017)
70. G. Inghirami et al., Eur. Phys. J. C **76**, 659 (2016)
71. G. Inghirami et al., Eur. Phys. J. C **80**, 293 (2020)
72. D.E. Kharzeev, H.J. Warringa, Phys. Rev. D **80**, 034028 (2009)
73. V. Roy, S. Pu, L. Rezzolla, D.H. Rischke, Phys. Rev. C **96**, 054909 (2017)
74. S. Pu, D.L. Yang, Phys. Rev. D **93**, 054042 (2016)
75. G.S. Bali, F. Bruckmann, G. Endrdi, A. Schäfer, Phys. Rev. Lett. **112**, 042301 (2014)
76. L.G. Pang, G. Endrodi, H. Petersen, Phys. Rev. C **93**, 044919 (2016)